Climate Dynamics (2021) 56:1251–1264
https://doi.org/10.1007/s00382-020-05531-9

Dominant modes of ensemble mean signal and noise in seasonal forecasts of SST

Zeng-Zhen Hu[1] · Arun Kumar[1] · Jieshun Zhu[1,2]

Received: 13 July 2020 / Accepted: 10 November 2020 / Published online: 3 January 2021

Abstract
In contrast to the temporal evolution of forecast ensemble mean (signal) and spread (noise) in an ensemble of seasonal forecasts, the spatial patterns of signal and noise components for sea surface temperature (SST) predictions have not been analyzed. In this work, we examine the leading patterns of signal and noise components of SST forecasts by the National Centers for Environmental Prediction Climate Forecast System version 2. It is noted that the leading empirical orthogonal function pattern of SST is similar between the signal and the noise with maximum loading in the central and eastern tropical Pacific associated with El Niño–Southern Oscillation (ENSO) variability. The similarity implies that while some members of the forecasts predict a stronger (weaker) ENSO than others, the dominant pattern of SST anomalies from all members still resembles the ENSO SST pattern. This reflects the notion that for each forecast ensemble member, the evolution of ENSO is governed by the similar air–sea coupled interactions, the strength of which, however, differs due to unpredictable noise. On the other hand, the leading mode of the signal and the noise are found temporally independent. Thus, it is concluded that although the largest variability in the signal and the noise is spatially collocated, their temporal evolution is independent.

Keywords Similar leading patterns · Signal and noise · Similar air–sea coupled interactions · CFSv2

1 Introduction

Short-term (monthly-interannual) climate predictions are now operational at many centers (O'Lenic et al. 2008; National Research Council 2010; Peng et al. 2012; Saha et al. 2014; MacLachlan et al. 2015; Johnson et al. 2019). This progress is largely attributed to the understanding of the El Niño–Southern Oscillation (ENSO) and its global impact (Rasmusson and Carpenter 1982; Ropelewski and Halpert 1987; Glantz 2000; National Research Council 2010; Hu et al. 2020), and further, our ability to skillfully predict sea surface temperature (SST) variations associated with ENSO (National Research Council 2010; Xue et al. 2013). SST predictions now rely more-and-more on the use of multiple comprehensive climate models and ensemble prediction techniques are utilized to estimate their forecast skill and uncertainty (Graham et al. 2011; Tompkins et al. 2017).

A well-known feature of ensemble prediction systems is an increase in ensemble spread with lead time (Molteni et al. 1996; Kumar and Hu 2014; Scaife and Smith 2018; Hu et al. 2019). In the context of ENSO prediction, quantification of associated uncertainty in the prediction is generally done in terms of now well-known "ENSO plume diagram" where the forecast amplitude of the Niño3.4 index [defined as SST anomalies (SSTAs) averaged in 5° S–5° N, 170° W–120° W] for individual forecasts in the ensemble is shown. An example of ENSO plume for the operational seasonal prediction system at the National Centers for Environmental Prediction—the Climate Forecast System version 2 (CFSv2) (Saha et al. 2014)—is shown in Fig. 1 as well as Figs. S1, S2 of Hu et al. (2019). As mentioned, a general feature of ENSO plumes is an increase in ensemble spread as forecast lead time increases, implying that some forecast members predict SSTAs larger than the ensemble mean while others predict SSTAs smaller than the ensemble mean.

The availability of ensemble forecasts allows for quantification of the predictable signal and the unpredictable noise. For example, ensemble mean (that highlights the

✉ Zeng-Zhen Hu
Zeng-Zhen.Hu@NOAA.GOV

[1] Climate Prediction Center, NCEP/NWS/NOAA, 5830 University Research Court, College Park, MD 20740, USA

[2] Earth System Science Interdisciplinary Center, The University of Maryland, College Park, MD 20740, USA

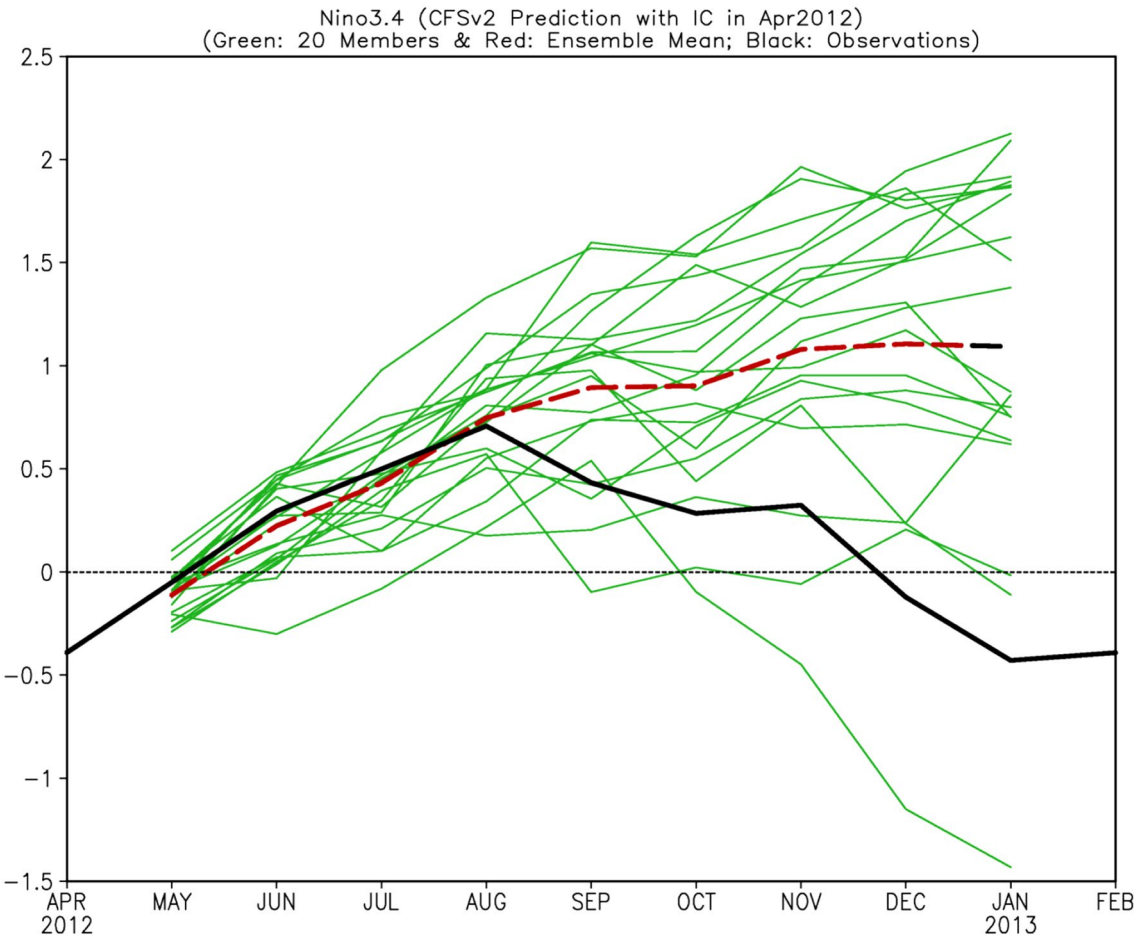

Fig. 1 Niño3.4 index predicted by the CFSv2 model with 20 different initial conditions in April 2012. The solid black line is the observation, dashed red line is the ensemble mean, and thin green lines are individual forecast members

commonality among individual forecast members) is the predictable signal while differences among individual forecasts from an ensemble are different renditions of noise (Kumar and Hoerling 2000). The noise varies from one forecast member to another. Knowledge of signal and noise components quantifies predictability that is measured by the signal-to-noise ratio (SNR). Small (large) SNR corresponds to lower (higher) predictability (Kumar and Hoerling 2000; Jha and Kumar 2009; Scaife and Smith 2018; Hu et al. 2019). As an example, Fig. 2 displays the lead-time and target month (the center month of 3-month average) dependent standard deviations of the ensemble mean and spread as well as SNR of the Niño3.4 index in the CFSv2 predictions. It shows that, for seasonal forecasts as an initial value problem, in addition to the dependence on seasons, signal and SNR are large and noise is small near the initial time of the forecast. With an increase in forecast lead-times, signal decreases, and noise increases, resulting in a smaller SNR (Peng et al. 2011). Consequently, forecast skill is also higher (lower) for shorter (longer) leads. This characteristic of SNR is evident in the example of ENSO plume (Fig. 1). It is also noted that the seasonality of SNR follows the well-known predictability feature of ENSO, that is, the lowest SNR values appear during the boreal spring, a reflection of the spring barrier in ENSO predictability. In contrast, the largest values for SNR occur in boreal fall and winter when the amplitude of ENSO SSTAs, on average, is also the largest.

To understand ENSO predictability, it is of interest to understand how the signal and the noise evolve with lead time, and further, what are their dominant spatial patterns? Some questions of importance in the context of understanding ENSO predictability are: are there similarities between the dominant modes of variability for signal and noise? How do signal and noise spatial patterns vary with forecast lead times? Are the dominant modes of signal and noise temporally independent? Understanding these questions is of importance for quantifying ENSO predictability, for its realization by prediction systems, and further, and for understanding the prediction differences across ensemble members.

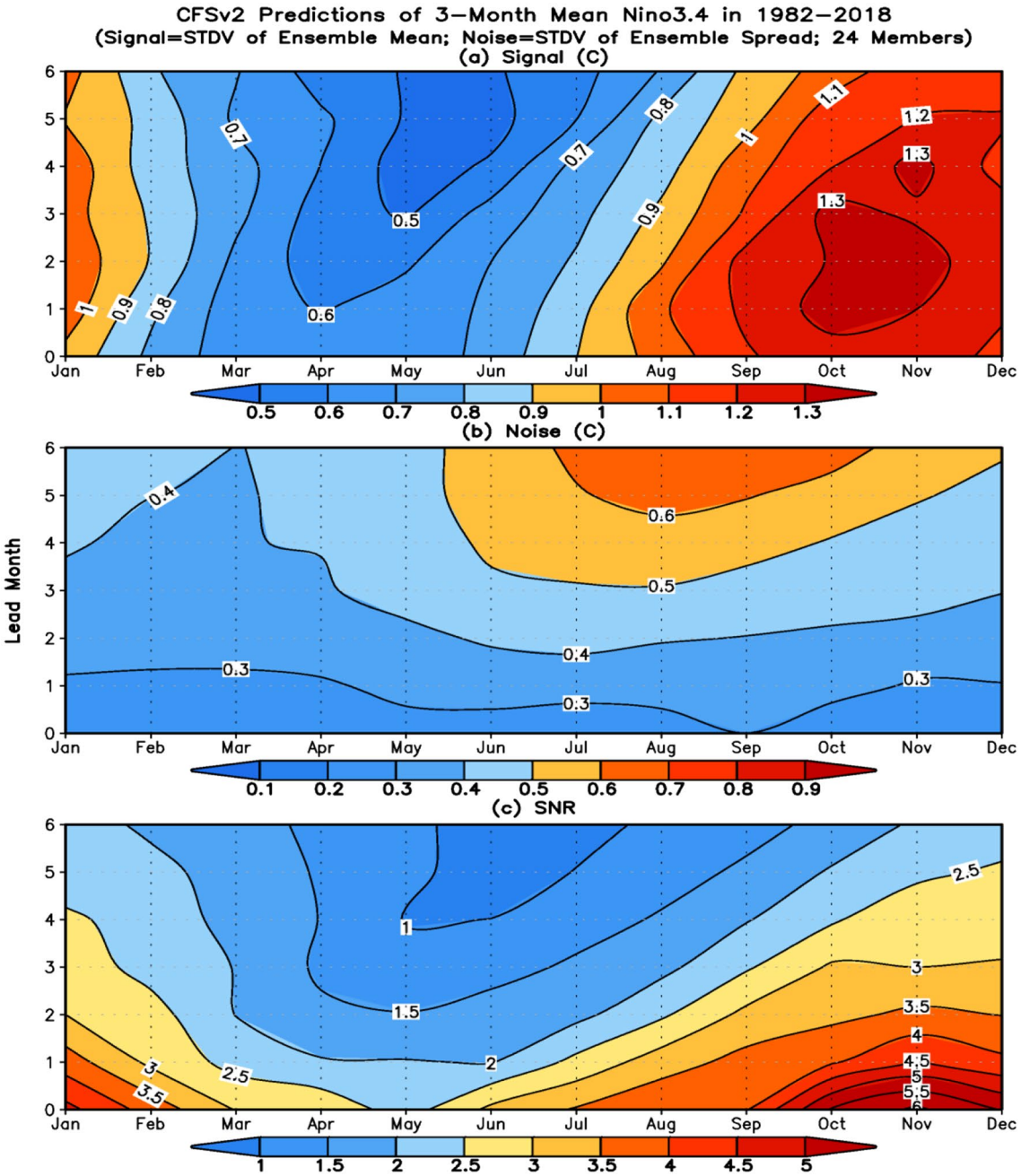

Fig. 2 Standard deviations of **a** ensemble mean (signal), **b** ensemble spread (noise), and **c** signal-to-noise ratio (SNR) of the Niño3.4 index in CFSv2 forecasts in 1982–2018 varied with target month in the center of 3-month average (x-axis) and lead time (y-axis). 20 ensemble members and a 3-month mean are used in the calculations

To understand the atmospheric predictability over North America, Peng et al. (2014) analyzed dominant modes of variability in the atmospheric signal and the noise by using an ensemble of forecasts. They noted that the dominant modes of the signal were like the dominant modes of noise variability. The analysis implied that the predictable (i.e., the signal) and unpredictable (i.e., the noise) components of atmospheric variability had similar spatial patterns. Their analysis also pointed to the validity of the argument that external forcing, by altering the characteristics of modes of noise (for example, the residence time in a particular phase), leads to predictable spatial patterns that also resemble the dominant spatial patterns of noise.

It has also been documented that the amplitude of forecast spread among individual forecast members in an ensemble is quasi-independent from event to event, and further, is

independent of the amplitude of the ensemble mean anomalies for both SST and atmospheric variables, such as geopotential height at 200 hPa (e.g., Kumar and Hoerling 1998; Kumar et al. 2000; Peng and Kumar 2005; Jha and Kumar 2009; Kumar and Hu 2014; Jha et al. 2019). In other words, due to the small variation of the noise amplitude, the interannual variations in SNRs are primarily determined by variation in the signal strength (ensemble mean anomaly amplitude) (Tang et al. 2005, 2008). Recently, Hu et al. (2019) noted that the prediction skill of an ENSO cycle varies with its phase that is linked to the variations of SNR, and primarily with the amplitude of the signal. In contrast, the noise, both in the Niño3.4 region and the entire Pacific Ocean, does not depend much on the Niño3.4 amplitude (Hu et al. 2019).

In the context of ENSO prediction and associated SSTs, although variations in the amplitude of signal and noise have been analyzed (Kumar et al. 2017; Kumar and Hu 2014), the characteristics of the spatial feature of SST prediction associated with the signal and the noise have not yet been assessed. In this work, to complement the analysis of Hu et al. (2019), we further examine the leading patterns of the signal and the noise in forecasts of global SSTs with the focus on the tropical Pacific from a seasonal forecast system. The variances explained by atmosphere–ocean coupling associated with the leading patterns of both the signal and the noise in the forecasts are further compared. The paper is organized as the following: the data used in this work are introduced in Sect. 2, the results are shown in Sect. 3, and the summary and discussion are given in Sect. 4.

2 Data and methods

The forecasts (both hindcasts and real-time forecasts) of SSTs and wind stress examined in this work are from CFSv2 (Xue et al. 2013; Saha et al. 2014). The analyzed forecasts in this work extend for 9 months with initial conditions (ICs) at 00Z, 06Z, 12Z, and 18Z of every 5 days starting January 1st. The hindcasts cover the period from January 1982 to December 2010, and real-time forecasts from January 2011 to 2018. Here, the 0-month lead forecast is referred to as forecasts initialized from the previous month. For example, the 0-month lead prediction of December refers to 20 predictions of the monthly means from ICs on November 7, November 12, November 17, November 22, and November 27 at 00Z, 06Z, 12Z, and 18Z. The ICs of both the ocean and atmosphere are from the NCEP Climate Forecast System Reanalysis (CFSR, Saha et al. 2010; Xue et al. 2011).

To eliminate the discontinuity caused by the biases in CFSR around 1998–99 (Xue et al. 2011; Kumar et al. 2012), two climatologies are used to compute the anomalies for the CFSv2 forecasts. The first one is the average between January 1982–December 1998, and the second one is the average between January 1999–December 2018. Also, all the monthly mean SST data are converted into 3-month seasonal means. Similar processing has also been used in previous studies (Xue et al. 2013; Hu et al. 2013, 2014, 2019; Kumar and Hu 2014).

The forecasts from 20 ICs in each month are used to construct the ensemble mean, which is referred to as "signal". The departure of individual forecasts in the ensemble from the ensemble mean (or the signal) is the "noise". The dominant mode of the signal is identified based on the empirical orthogonal function (EOF) of ensemble mean predictions of SSTAs. Similarly, the dominant mode of noise is identified by applying EOF to SSTAs departures in individual forecasts from the ensemble mean. In the EOF analyses, covariance matrices of forecast SSTAs over the global ocean for a specific lead time are calculated. To have identical data length between the signal and the noise, a randomly selected ensemble member from each year is used for the calculation of the departure from the ensemble mean to represent the noise component.

To verify the results based on the CFSv2 hindcasts, we also conducted EOF analyses for the SSTA forecasts with five other models (GEM_NEMO, NASA GEOS5v2, CanCM4i, GFDL_FLOR; and NCAR_CCSM4) from the North American Multi-Model Ensemble (NMME; Kirtman et al. 2014). The EOF analyses are applied separately for the ensemble mean (signal) and the departure of one randomly picked member from the ensemble mean (noise) of each model. The analyzed forecasts are the 3-month lead with initial conditions during January 1982–December 2016. The ensemble member size used in this work is 4 for NCAR_CCSM4, 24 for GFDL_FLOR, and 10 for the other models.

Observed SST and surface wind stress data are from the reanalyses from the National Center for Environmental Prediction Global Ocean Data Assimilation System from January 1979 to the present (GODAS; Behringer 2007). In GODAS, both oceanic temperature and synthetic salinity profiles are assimilated in a 3DVAR scheme. There are 40 vertical levels in the model together with a $1^\circ \times 1^\circ$ resolution (enhanced to 1/3 by 1/3° within 10° of the equator). In GODAS, the third version of Modular Ocean Model (MOM3) is forced by the momentum flux, heat flux, and freshwater flux from the NCEP/the U. S. Department of Energy Reanalysis (NCEP/DOE; Kanamitsu et al. 2002).

Observed precipitation data are from the monthly Climate Prediction Center (CPC) Merged Analysis of Precipitation (CMAP; Xie and Arkin 1997). The CMAP precipitation is obtained based on satellite estimates and gauge data and blended with the NCEP/the National Center for Atmospheric Research (NCEP/NCAR) precipitation values (Kalnay et al. 1996). The CMAP precipitation data are at a $2.5^\circ \times 2.5^\circ$ global resolution and span January 1979 to the present.

3 Results

Figure 3a and b show the dominant EOF pattern (EOF1) for the variability of the signal and the noise for the 3-month lead forecasts, which explains 30% of the total signal variance and 7% of the total noise variance, respectively. Here, the signal (noise) variance is defined as the variance of ensemble mean (departure from the ensemble mean) variability. The major loadings in Fig. 3b, c are confined to the central and eastern tropical Pacific, and the loadings are small in the other ocean basins, suggesting that the dominant modes (EOF1) of both the signal and the noise may be associated with ENSO variability. This is confirmed by their spatial patterns of correlation between the Niño3.4 index and total (signal + noise) SSTAs (Fig. 4a), and the corresponding correlation spatial patterns between PC1 of the signal and total SSTA (Fig. 4b), between PC1 of the noise and total SSTA (Fig. 4c), and between PC1 of the noise and the noise portion of SSTA (Fig. 4d) in the forecasts. For the temporal variations, the first principal component (PC1) of the signal variability is highly correlated with the observed Niño3.4 index with a correlation coefficient of 0.84. On the other hand, the

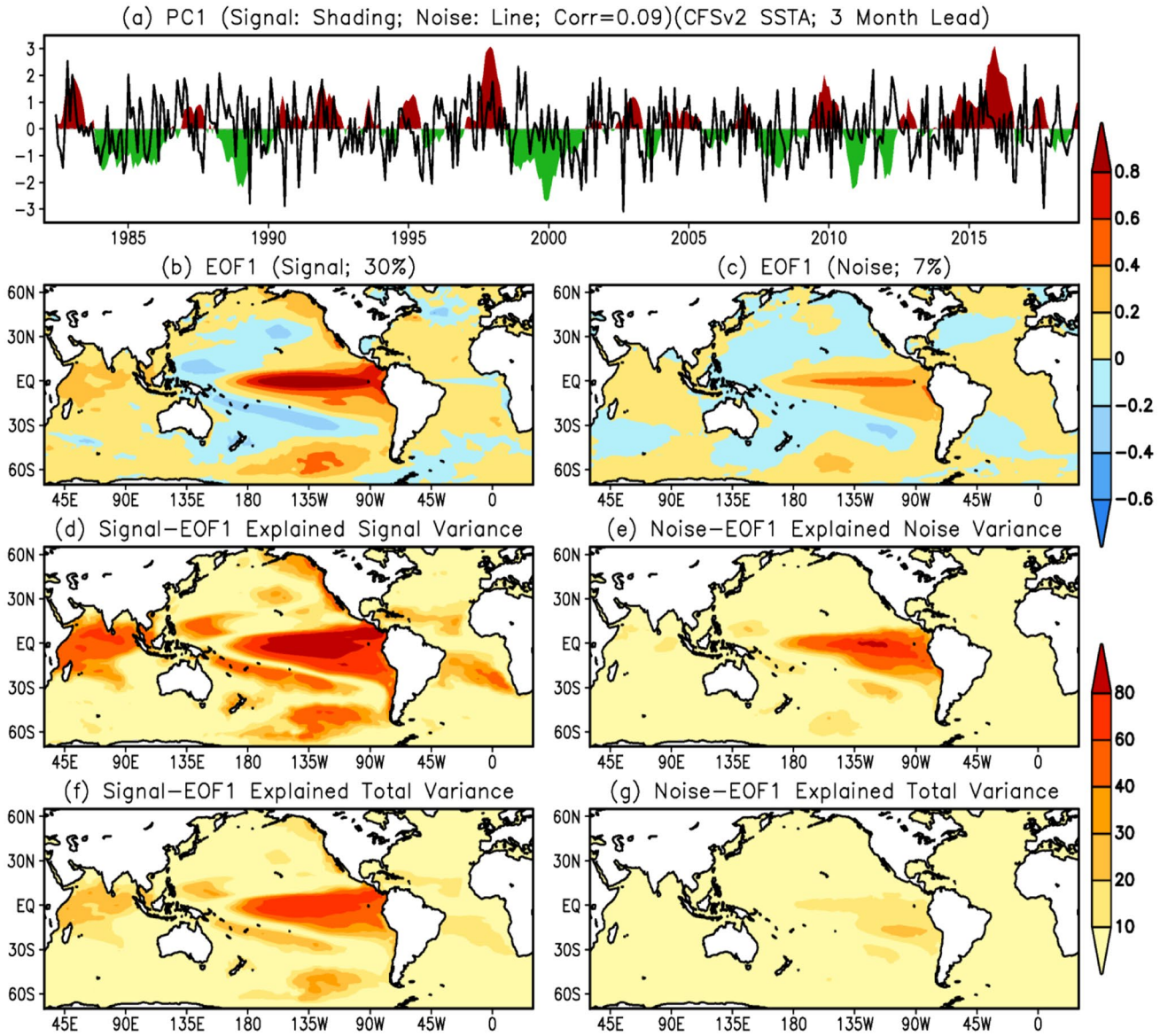

Fig. 3 EOF analysis of SSTAs forecast at the 3-month lead. PC1 of the signal (ensemble mean; shading) and the noise (ensemble spread; curve) (**a**); EOF1 of the signal (**b**); EOF1 of the noise (**c**); ratio (%) of signal variance explained by EOF1 of signal (**d**); ratio of noise variance explained by EOF1 of noise (**e**); ratios of total variance (signal + noise) explained by EOF1 of signal (**f**) and by EOF1 of noise (**g**). The correlation between PC1 of the signal and the noise is 0.09

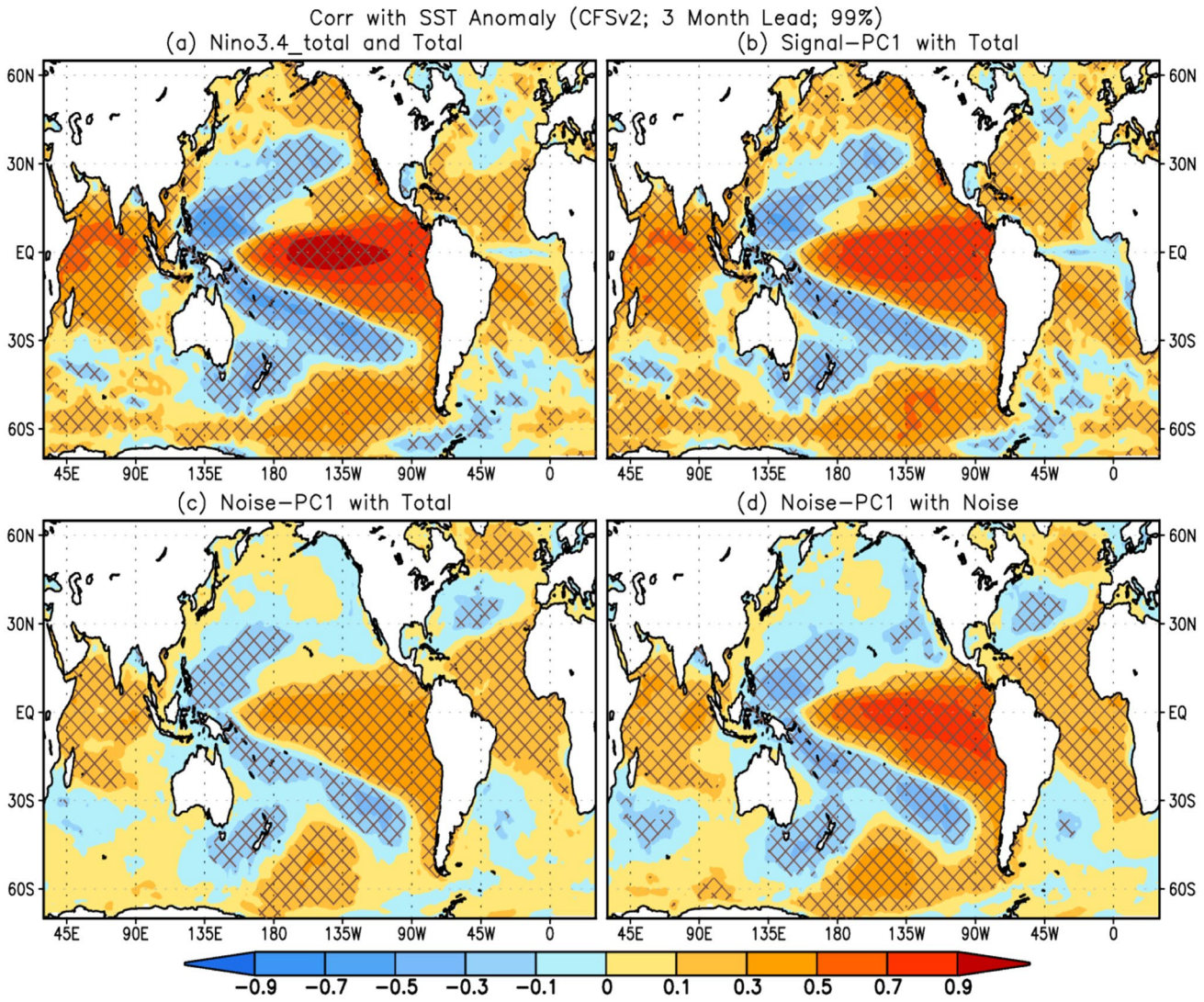

Fig. 4 3-month lead forecasts: correlations between Niño3.4 index and SSTAs (**a**), between PC1 of signal and SSTAs (**b**), between PC1 of noise and SSTAs (**c**), and between PC1 of noise and SSTA of noise (**d**). The hatches indicate significant correlations at 1% level based on a t test

correlation of PC1 of the noise with the observed Niño3.4 index is 0.09, confirming the lack of temporal coherence between PC1 of the noise and the Niño3.4 index. We note that repeated calculations of the noise with a different selection of individual ensemble members (not shown) gave almost identical results, suggesting the robustness of the leading mode of the noise.

Next, we compute the fraction of SSTA variability that is explained by EOF1 of the signal and the noise. The variability associated with signal and noise PC1 is computed by multiplying the corresponding EOF1 pattern with respective PC1 and then computing the variance over the years. Regionally, EOF1 of the signal explains more than 60% of the variance of the overall signal variability in the central and eastern tropical Pacific as well as in the tropical Indian Ocean, while the explained fraction in the tropical Atlantic is smaller and reaches only about 40% in a few areas (Fig. 3d). This is consistent with the correlations shown in Fig. 4a and also the fact that co-variability in the Indian Ocean associated with ENSO is stronger than that in the Atlantic Ocean associated with ENSO (e.g., Frauen and Dommenget 2012). The fractions of the variance of total SSTAs explained by EOF1 of the signal are smaller with maximum values of 40–60% in the central and eastern tropical Pacific (Fig. 3f).

Compared to the signal, EOF1 of the noise explains a smaller fraction of the total noise variance (Fig. 3e, g). For example, approximately 40% of noise variance is explained by EOF1 of noise in the central and eastern tropical Pacific, with less than 30% variance explained in the tropical Indian Ocean and less than 10% in the Atlantic Ocean (Fig. 3e). For the total variance, the explained fraction by EOF1 of the noise is even smaller (mostly less than 30%), with a

maximum located in the central and eastern tropical Pacific (Fig. 3g). Such differences between the EOF1 of the signal and noise suggest that the signal is more spatially and temporally coherent than the noise.

Contrary to EOF1, EOF2 of the signal and the noise explain a much smaller fraction (12% of the signal variance and 4% of the noise variance for the 3-month lead forecasts, respectively) (Fig. 5). Compared with that of the signal EOF, the percentages of the total noise variance explained by individual EOFs decline slower with increasing EOF number. The maximum fractions of the explained variance by EOF2 for both the signal and the noise are mainly in the off-equatorial regions. Therefore, the analysis here focuses on EOF1 only.

To address the question of how the dominant modes of variability in the signal and the noise change with lead times, we repeated the EOF analysis for SST forecasts for 6-month and 0-month (not shown) leads. The results of the forecasts at the 6-month and 0-month leads are similar to that of the forecasts of the 3-month lead shown in Figs. 3 and 4. Such similarity reflects a basic feature that leading variability patterns of the signal and the noise are similar for different lead times, which is also similar to the dominant mode of the observed SST variability in the central and eastern tropical Pacific associated with ENSO. The similarity of the leading modes of the signal and the noise suggests that while some forecast members predict a stronger/weaker ENSO than others, the intra-ensemble difference may still be a reflection of coupled interactions similar to that are responsible for ENSO variability. Also, although the amplitudes of EOF1 of the noise increase with lead times, there are little changes in the spatial pattern between different lead times.

Contrary to the similarity of the spatial patterns of the leading modes of the signal and the noise, their temporal evolution is largely independent. The correlation between PC1 of the signal and the noise is 0.07 for the 6-month lead (not shown), 0.09 for the 3-month lead (Fig. 3a), and − 0.06 for the 0-month lead (not shown). That is consistent with previous work (e.g., Kumar and Hoerling 1998; Kumar et al. 2000; Tang et al. 2005, 2008; Jha and Kumar 2009;

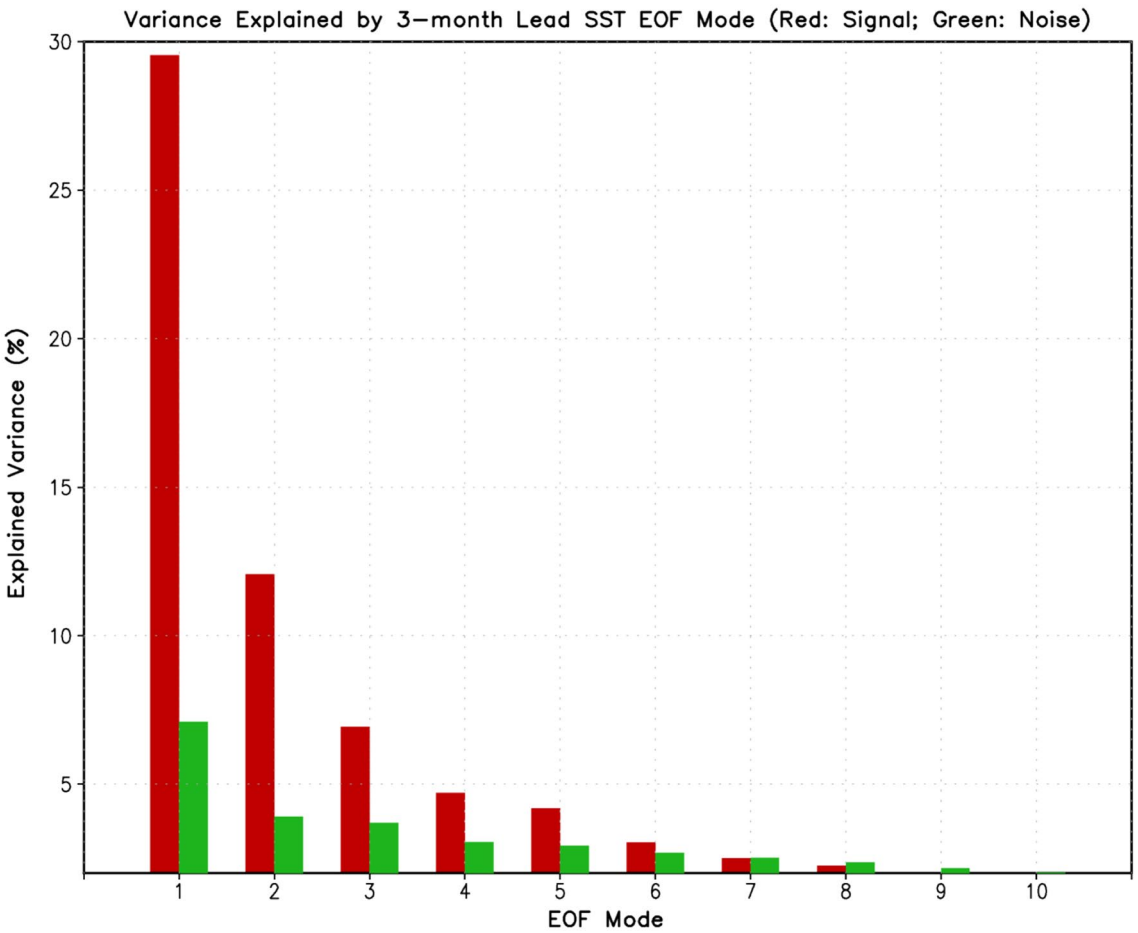

Fig. 5 Percentages of total signal (noise) variance explained by the first 10 EOF modes of the signal (noise) of the CFSv2 predicted SSTA at the 3-month lead. The red (green) bars are for the signal (noise)

Kumar and Hu 2014; Jha et al. 2019; Hu et al. 2019) that the amplitude of the noise has no systematic dependence on the predicable signal. Since PC1 for the signal (shading; Fig. 3a) represents the interannual variability of ENSO (see Fig. 18 of Xue et al. 2011), it is concluded that the large variability in both the signal and the noise are collocated spatially and associated with ENSO, but their temporal evolution is independent.

The spatial distribution of the leading modes of both the signal and noise in the tropical Pacific (Fig. 3b, c) is similar to that of the corresponding total variance. As an example, Fig. 6 shows the variance of signal, and noise, as

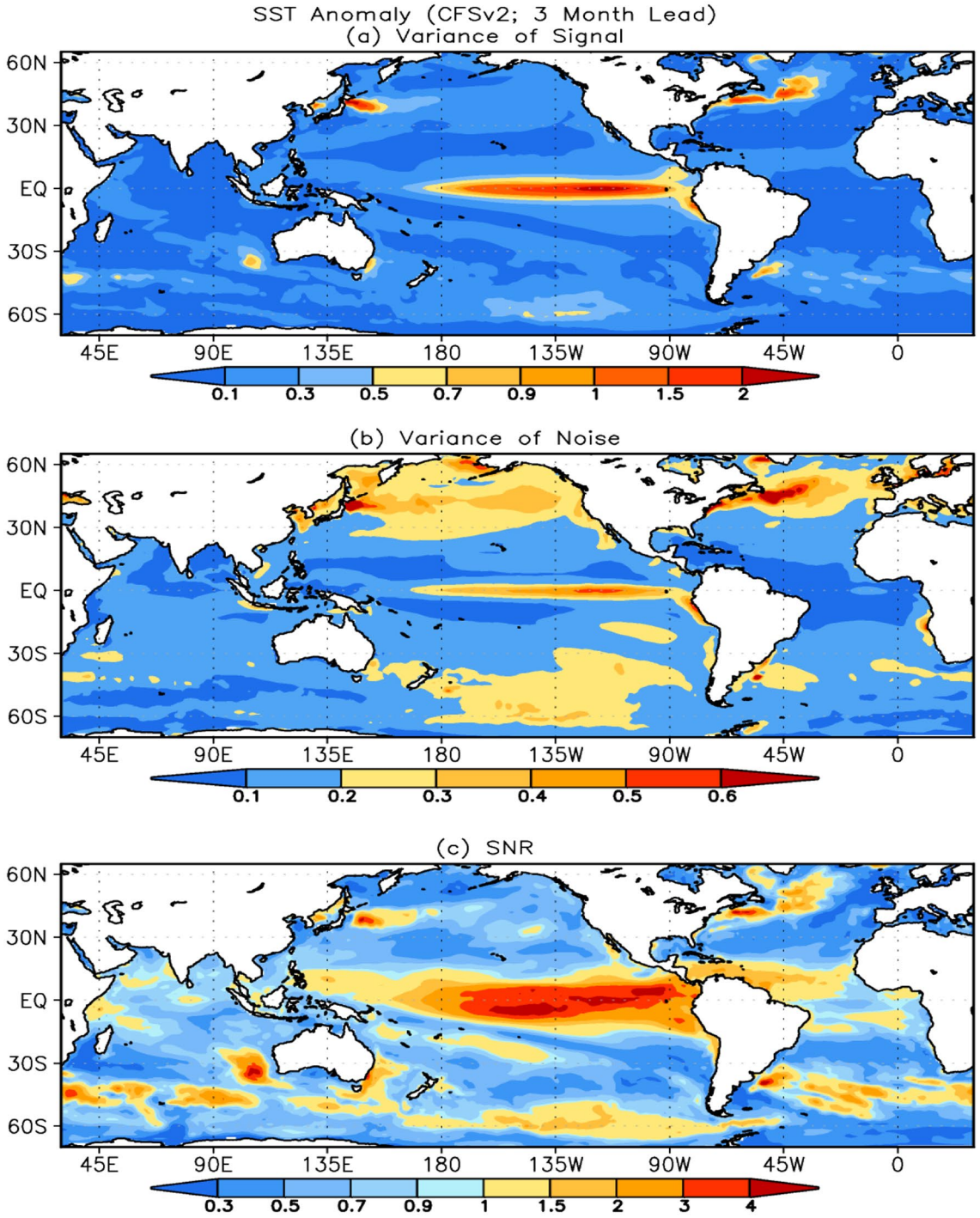

Fig. 6 Variances of **a** ensemble mean and **b** spread of SSTAs forecast at the 3-month lead of the CFSv2 forecasts in January 1982–December 2018, and **c** ratio of **a** to **b**. **a** and **b** are referred to as signal and noise, respectively, and **c** is the signal-to-noise ratio. The unit is $(°C)^2$ in **a**, **b**

well as signal-to-noise ratio (SNR) for the 3-month lead predictions. Large variance centers of the noise appear in the central and eastern tropical Pacific, as well as the middle and high latitudes. The pronounced noise variance in the middle and high latitudes may reflect challenges to forecast variations related to the jet stream and/or storm track that modulate the underlying SST variability. In contrast, the largest variance of the signal is confined in the central and eastern tropical Pacific, which corresponds to the maximum signal-to-noise ratio (SNR; Fig. 6c), reflecting the large predictability, and potentially high prediction skills (e.g., Kumar and Hoerling 2000; Scaife and Smith 2018).

The large SNR in the central and eastern tropical Pacific is collocated with atmospheric and oceanic coupling which is quantified here by co-variances of SSTA with precipitation anomalies in the observation and the CFSv2 forecast of the 20-member ensemble mean (signal) and in the departure of one randomly chosen member from the ensemble mean (noise) at 3-month lead (Fig. 7a, b). Consistent with previous work (such as Fig. 3a of Wu et al. 2006), the positive covariance is seen in the central and eastern tropical Pacific associated with ENSO in both the observation and ensemble mean of the CFSv2 forecast (Fig. 7). Such large positive covariance in the central and eastern tropical Pacific implies that the SSTA in the region is largely driven by ocean dynamic processes. Interestingly, for the noise (Fig. 7b), the spatial distribution pattern of the co-variance is similar to that of the observation (Fig. 7c) and the ensemble mean (Fig. 7a) with the maximum in the central and eastern tropical Pacific, although the amplitude is reduced.

The atmospheric and oceanic positive feedback associated with ENSO can be estimated by the so-called atmospheric Bjerknes feedback, which can be quantified by the linear regression of zonal wind stress anomaly onto the Niño3.4 index (Fig. 8) (Lloyd et al. 2009; Bellenger et al. 2014; Li et al. 2019). We can see from Fig. 8 that the regression pattern in the tropical Pacific is similar between the observations (GODAS) and one randomly chosen member of the CFSv2 predictions at different lead-times (shading in Fig. 8). However, there are profound differences in the strength of the positive feedback between the observations and the CFSv2 predictions (contours in Fig. 8b–d). Thus, the spatial similarity of the leading modes between the noise and ensemble mean (and/or observation) may imply that to some extent, both the signal and noise in the central and eastern tropical Pacific are driven by similar atmosphere and ocean coupling processes. In other words, due to stochastic variability and model biases, some members of the forecasts overestimate the coupling strength while some others underestimate it (Larson and Kirtman 2015, 2017). Both lead to the spread of the forecasts among the individual members and result in the departure from the ensemble mean, and as a result, the spatial pattern of the leading mode of both the signal and noise are found to be similar.

4 Summary and discussion

Previous results have documented that forecast spread among individual ensemble members is quasi-independent to the amplitude of the ensemble mean anomalies (e.g., Kumar and Hu 2014; Hu et al. 2019). This independence of the temporal evolution of the signal and the noise amplitude in climate forecast implies that year-to-year variations in predictability are mainly determined by the signal (ensemble mean) rather than variations in the amplitude of the noise (model spread) (Kumar et al. 2000; Kumar and Hoerling 2000; Tang et al. 2005, 2008). However, compared to the well documented temporal evolutions, the possible relationship of the spatial variations between the signal and the noise has not been well examined.

In this work, to complement Hu et al. (2019), we further examine the leading spatial patterns of ensemble mean (signal) and spread (noise) variability in the forecasts of NCEP CFSv2. It is shown that a similar leading EOF pattern is present in the signal and the noise EOF analyses. The major loading is confined in the central and eastern tropical Pacific which is associated with the ENSO variability. The results are similar for different lead times. The similarity of the leading modes of the signal and the noise implies that some individual members of the forecasts predict a stronger or weaker ENSO than others, and the coupled atmosphere–ocean processes in the central and eastern tropical Pacific that lead to the intra-ensemble variations may be similar to the ENSO dynamics. The result also highlights the limits in ENSO predictability and prediction skill in an atmosphere–ocean coupled forecast system. In an ensemble forecast system, small perturbations that mimic various uncertainties in initial conditions, via coupled air–sea interactions similar to ENSO, can lead to different outcomes for ENSO prediction in individual forecasts, as encapsulated in the ENSO plume diagrams (Fig. 1).

Although the leading patterns of the signal and the noise are similar, their temporal evolutions are independent, meaning that despite coherent spatial variations in the central and eastern tropical Pacific are present in both the signal and the noise, their temporal variabilities are independent. This suggests that departures in individual members from the ensemble mean are distributed randomly around the ensemble mean and are not biased towards a particular phase of ENSO in the ensemble mean. Moreover, the leading pattern of the signal explains much larger fractions of total SST variability than that of the noises. Such differences may imply that variations of the signal are more coherent spatially and temporally than the variations of the noise.

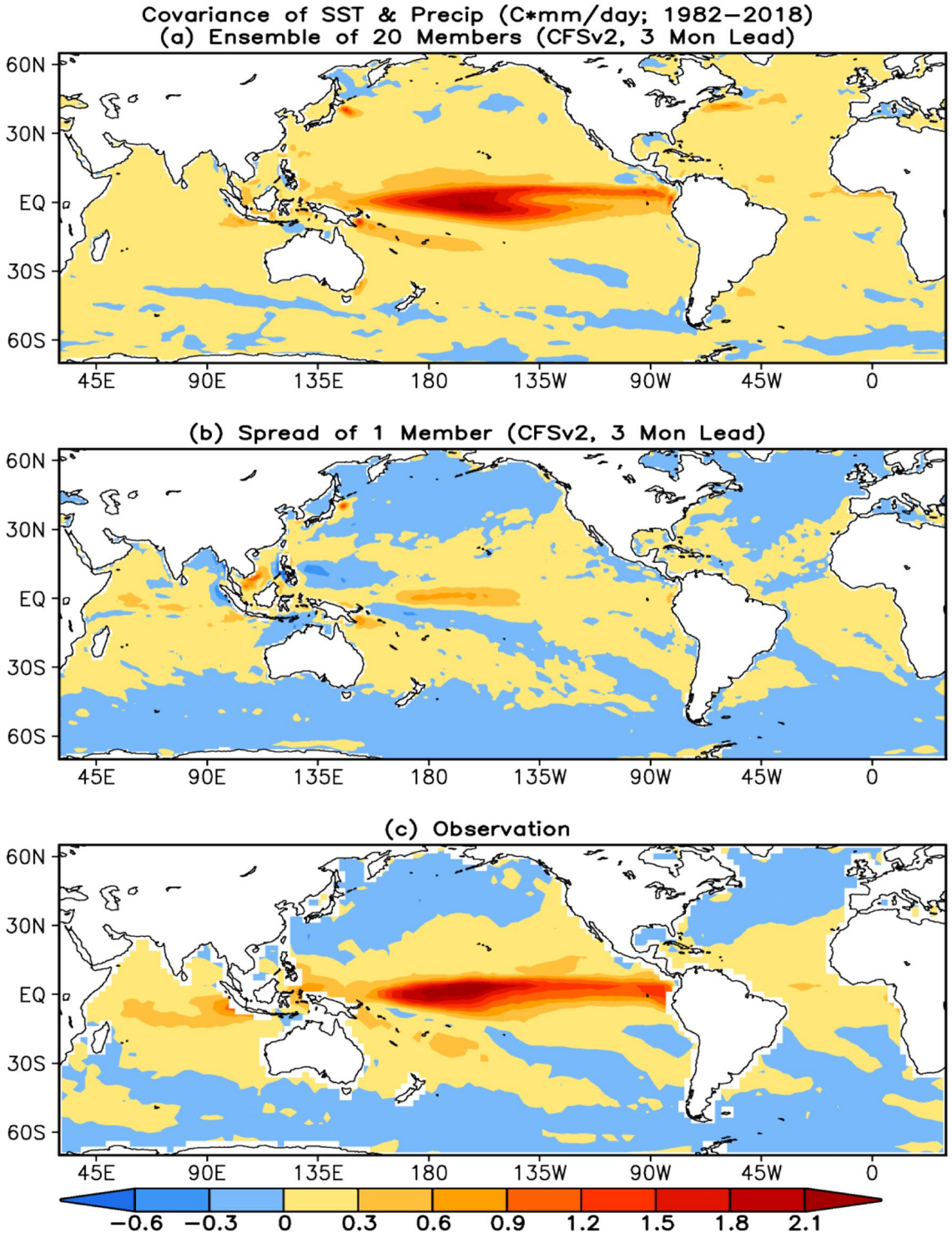

Fig. 7 Pointwise and simultaneous covariance of SSTA with precipitation of **a** ensemble mean of 20 members, **b** one member in the CFSv2 forecasts, and **c** observations during January 1982–December 2018. The unit is °C mm/day

The spatial distribution similarity and temporal evolution independence of the leading modes of signal and noise of SSTAs based on forecasts from CFSv2 are further verified by the corresponding EOF analyses of five models from NMME (Fig. 9). Although there are some differences in details among the models, the main loading of the EOF1 of both the signal and noise are in the tropical

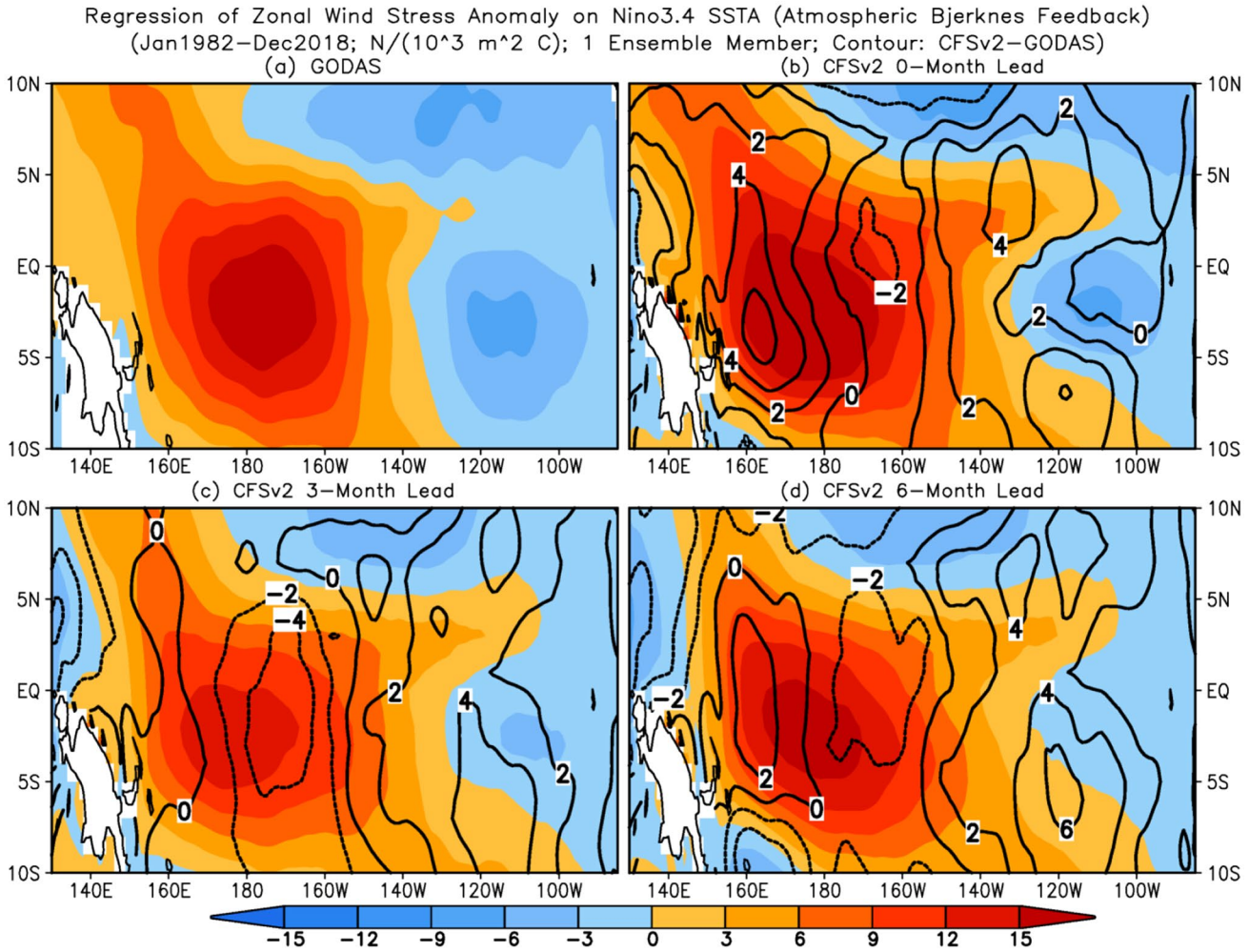

Fig. 8 The atmospheric Bjerknes feedback: Linear regression of zonal wind stress anomaly onto the Niño3.4 index in January 1982-December 2018. Shading: **a** GODAS, 0-month (**b**), 3-month (**c**), and 6-month (**d**) lead predictions of CFSv2 (one member). The contours in **b**–**d** are the differences between the corresponding CFSv2 and GODAS. The unit is N/(10^3 m^2 °C) for the shading and the contour interval is 2 N/(10^3 m^2 °C)

Pacific associated with ENSO, and their corresponding PC1 of the signal and noise have no significant correlation.

The similarity of the leading EOF patterns between the signal and noise was derived based on global SST with the focus on the tropical Pacific. Nevertheless, the conclusions about the leading pattern of signal and noise in the extratropics may be different. This might be associated with the different characteristics of the climate in the tropics and extratropics, as well as the ability of climate model in predicting them. For example, Eade et al. (2014) argued that for the climate variability in the North Atlantic, the predictable component in models is sometimes lower than in observations with each ensemble member containing too much noise.

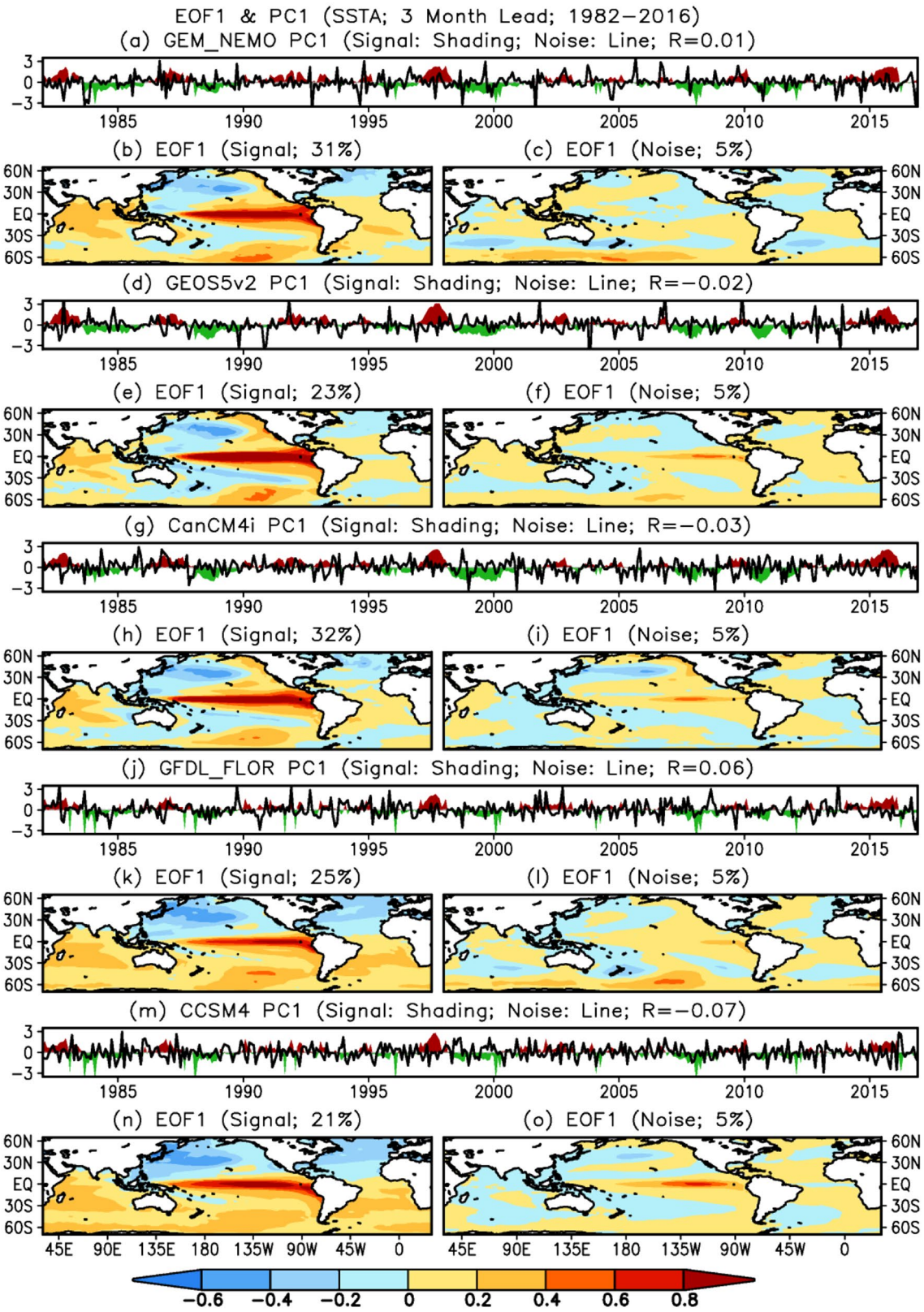

Fig. 9 EOF1 and PC1 of predicted global SSTAs at the 3-month lead for the ensemble mean (signal) and departure of one member from their ensemble mean (noise) with initial conditions in January 1982–December 2016. **a**–**c** GEM_NEMO; **d**–**f** NASA GEOS5v2; **g**–**i** CanCM4i; **j**–**l** GFDL_FLOR; and **m**–**o** NCAR_CCSM4. The values of R represent the correlations of the PC1 between the signal and noise. The percentages of the variance explained by EOF1 are shown in the subtitles

Acknowledgements The authors appreciate the constructive comments from Dr. V. Krishnamurthy and two anonymous reviewers which help us to improve the paper significantly. The scientific results and conclusions, as well as any view or opinions expressed herein, are those of the authors and do not necessarily reflect the views of NWS, NOAA, or the Department of Commerce.

References

Behringer DW (2007) The Global Ocean Data Assimilation System (GODAS) at NCEP. In: Preprints, 11th symposium on integrated observing and assimilation systems for atmosphere, oceans, and land surface, San Antonio, TX, Amer. Meteor. Soc., 3.3. http://ams.confex.com/ams/87ANNUAL/techprogram/paper_119541.htm. Accessed 16 Jan 2007

Bellenger H, Guilyardi E, Leloup J, Lengaigne M, Vialard J (2014) ENSO representation in climate models: from CMIP3 to CMIP5. Clim Dyn 42(7–8):1999–2018. https://doi.org/10.1007/s00382-013-1783-z

Eade R, Smith D, Scaife A, Wallace E, Dunstone N, Hermanson L, Robinson N (2014) Do seasonal-to-decadal climate predictions underestimate the predictability of the real world? Geophys Res Lett 41:5620–5628. https://doi.org/10.1002/2014GL061146

Frauen C, Dommenget D (2012) Influences of the tropical Indian and Atlantic Oceans on the predictability of ENSO. Geophys Res Lett 39:L02706. https://doi.org/10.1029/2011GL050520

Glantz MH (2000) Currents of change: impacts of El Niño and La Niña on climate and society. Cambridge University Press, Cambridge, p 266

Graham R et al (2011) Long-range forecasting and global framework for climate services. Clim Res 47:47–55. https://doi.org/10.3354/cr00963

Hu Z-Z, Kumar A, Huang B, Wang W, Zhu J, Wen C (2013) Prediction skill of monthly SST in the North Atlantic Ocean in NCEP climate forecast system version 2. Clim Dyn 40(11–12):2745–2756. https://doi.org/10.1007/s00382-012-1431-z

Hu Z-Z, Kumar A, Huang B, Zhu J, Guan Y (2014) Prediction skill of North Pacific variability in NCEP climate forecast system version 2: impact of ENSO and beyond. J Clim 27(11):4263–4272. https://doi.org/10.1175/JCLI-D-13-00633.1

Hu Z-Z, Kumar A, Zhu J, Peng P, Huang B (2019) On the challenge for ENSO cycle prediction: an example from NCEP climate forecast system version 2. J Clim 32(1):183–194. https://doi.org/10.1175/JCLI-D-18-0285.1

Hu Z-Z, Kumar A, Jha B, Huang B (2020) How much of monthly mean precipitation variability over global land is associated with SST anomalies? Clim Dyn 54(1–2):701–712. https://doi.org/10.1007/s00382-019-05023-5

Jha B, Kumar A (2009) A comparative analysis of change in the first and second moment of the PDF of seasonal means with ENSO SSTs. J Clim 22:1412–1423. https://doi.org/10.1175/2008JCLI2495.1

Jha B, Kumar A, Hu Z-Z (2019) An update on the estimate of predictability of seasonal mean atmospheric variability using North American Multi-Model Ensemble. Clim Dyn 53(12):7397–7409. https://doi.org/10.1007/s00382-016-3217-1

Johnson SJ et al (2019) SEAS5: the new ECMWF seasonal forecast system. Geosci Model Dev 12(3):1087–1117. https://doi.org/10.5194/gmd-12-1087-2019

Kalnay E et al (1996) The NCEP/NCAR 40-year reanalysis project. Bull Amer Meteorol Soc 77:437–471

Kanamitsu M, Ebisuzaki W, Woollen J, Yang S-K, Hnilo JJ, Fiorino M, Potter GL (2002) NCEP-DOE AMIP-II reanalysis (R-2). Bull Am Meteorol Soc 83:1631–1643. https://doi.org/10.1175/BAMS-83-11-1631

Kirtman BP et al (2014) The North American multimodel ensemble: phase-1 seasonal-to-interannual prediction; phase-2 toward developing intraseasonal prediction. Bull Am Meteorol Soc 95:585–601

Kumar A, Hoerling MP (1998) Annual cycle of Pacific/North American seasonal predictability associated with different phases of ENSO. J Clim 11:3295–3308. https://doi.org/10.1175/1520-0442(1998)011%3c3295:ACOPNA%3e2.0.CO;2

Kumar A, Hoerling MP (2000) Analysis of a conceptual model of seasonal climate variability and implications for seasonal prediction. Bull Am Meteorol Soc 81:255–264. https://doi.org/10.1175/1520-0477(2000)081%3c0255:AOACMO%3e2.3.CO;2

Kumar A, Hu Z-Z (2014) How variable is the uncertainty in ENSO sea surface temperature prediction? J Clim 27(7):2779–2788. https://doi.org/10.1175/JCLI-D-13-00576.1

Kumar A, Barnston AG, Peng P, Hoerling MP, Goddard L (2000) Changes in the spread of the variability of the seasonal mean atmospheric states associated with ENSO. J Clim 13:3139–3151. https://doi.org/10.1175/1520-0442(2000)013%3c3139:CITSOT%3e2.0.CO;2

Kumar A, Chen M, Zhang L, Wang W, Xue Y, Wen C, Marx L, Huang B (2012) An analysis of the nonstationarity in the bias of sea surface temperature forecasts for the NCEP climate forecast system (CFS) version 2. Mon Weather Rev 140:3003–3016. https://doi.org/10.1175/MWR-D-11-00335.1

Kumar A, Hu Z-Z, Jha B, Peng P (2017) Estimating ENSO predictability: based on multi-model hindcasts. Clim Dyn 48(1–2):39–51. https://doi.org/10.1007/s00382-016-3060-4

Larson SM, Kirtman BP (2015) Revisiting ENSO coupled instability theory and SST error growth in a fully coupled model. J Clim 28:4724–4742. https://doi.org/10.1175/JCLI-D-14-00731.1

Larson SM, Kirtman BP (2017) Drivers of coupled model ENSO error dynamics and the spring predictability barrier. Clim Dyn 48:3631–3644. https://doi.org/10.1007/s00382-016-3290-5

Li X, Hu Z-Z, Huang B (2019) Contributions of atmosphere-ocean interaction and low-frequency variation to intensity of strong El Niño events since 1979. J Clim 32(5):1381–1394. https://doi.org/10.1175/JCLI-D-18-0209.1

Lloyd J, Guilyardi E, Weller H, Slingo J (2009) The role of atmosphere feedbacks during ENSO in the CMIP3 models. Atmos Sci Lett 10:170–176. https://doi.org/10.1175/JCLI-D-11-00178.1

MacLachlan C et al (2015) Global seasonal forecast system version 5 (GloSea5): a high-resolution seasonal forecast system. Q J R Meteorol Soc 141:1072–1084. https://doi.org/10.1002/qj.2396

Molteni F, Buizza R, Palmer TN, Petroliagis T (1996) The ECMWF ensemble prediction system: methodology and validation. Q J R Meteorol Soc 122:73–119

National Research Council (2010) Assessment of Intraseasonal to Interannual Climate Prediction and Predictability. The National Academies Press, Washington, DC (**ISBN-10: 0-309-15183-X**)

O'Lenic EA, Unger DA, Halpert MS, Pelman KS (2008) Developments in operational long-range climate prediction at CPC. Weather Forecast 23:496–515. https://doi.org/10.1175/2007WAF2007042.1

Peng P, Kumar A (2005) A large ensemble analysis of the influence of tropical SSTs on seasonal atmospheric variability. J Clim 15:1068–1085

Peng P, Kumar A, Wang W (2011) An analysis of seasonal predictability in coupled model forecasts. Clim Dyn 36:419–430

Peng P, Kumar A, Halpert MS, Barnston AG (2012) An analysis of CPC's operational 0.5-month lead seasonal outlooks. Weather Forecast 27:898–917. https://doi.org/10.1175/WAF-D-11-00143.1

Peng P, Kumar A, Jha B (2014) Climate mean, variability and dominant patterns of the Northern Hemisphere wintertime mean

atmospheric circulation in the NCEP CFSv2. Clim Dyn 42:2783–2799. https://doi.org/10.1007/s00382-014-2116-6

Rasmusson EM, Carpenter TH (1982) Variations in tropic is surface temperature and surface wind fields associated with the Southern Oscillation/El Niño. Mon Weather Rev 110:354–384

Ropelewski CF, Halpert M (1987) Global and regional scale precipitation patterns associated with the El Niño–Southern Oscillation. Mon Weather Rev 115:1606–1626. https://doi.org/10.1175/1520-0493(1987)115%3c1606:GARSPP%3e2.0.CO;2

Saha S et al (2010) The NCEP climate forecast system reanalysis. Bull Am Meteorol Soc 91:1015–1057. https://doi.org/10.1175/2010BAMS3001.1

Saha S et al (2014) The NCEP climate forecast system version 2. J Clim 27:2185–2208. https://doi.org/10.1175/JCLI-D-12-00823.1

Scaife AA, Smith D (2018) A signal-to-noise paradox in climate science. NPJ Clim Atmos Sci 1:28. https://doi.org/10.1038/s41612-018-0038-4

Tang Y, Kleeman R, Moore AM (2005) Reliability of ENSO dynamical predictions. J Atmos Sci 62:1770–1791. https://doi.org/10.1175/JAS3445.1

Tang Y, Lin H, Moore AM (2008) Measuring the potential predictability of ensemble climate predictions. J Geophys Res. https://doi.org/10.1029/2007JD008804

Tompkins AM et al (2017) The climate-system historical forecast project: providing open access to seasonal forecast ensembles from centers around the globe. Bull Am Meteorol Soc 98:2293–2301. https://doi.org/10.1175/BAMS-D-16-0209.1

Wu R, Kirtman BP, Pegion K (2006) Local air–sea relationship in observations and model simulations. J Clim 19:4914–4932. https://doi.org/10.1175/JCLI3904.1

Xie P, Arkin PA (1997) Global precipitation: a 17-year monthly analysis based on gauge observations, satellite estimates, and numerical model outputs. Bull Am Meteorol Soc 78:2539–2558

Xue Y, Huang B, Hu Z-Z, Kumar A, Wen C, Behringer D, Nadiga S (2011) An assessment of oceanic variability in the NCEP climate forecast system reanalysis. Clim Dyn 37(11–12):2511–2539. https://doi.org/10.1007/s00382-010-0954-4

Xue Y, Chen M, Kumar A, Hu Z-Z, Wang W (2013) Prediction skill and bias of tropical Pacific sea surface temperatures in the NCEP climate forecast system version 2. J Clim 26(15):5358–5378. https://doi.org/10.1175/JCLI-D-12-00600.1